ACS APPLIED MATERIALS & INTERFACES

Research Article

www.acsami.org

Electrospun TiO_2 Fiber Composite Photoelectrodes for Water Splitting

D. Regonini,*[,†] A. C. Teloeken,[‡] A. K. Alves,[‡] F. A. Berutti,[‡] K. Gajda-Schrantz,[†] C. P. Bergmann,[‡] T. Graule,[†] and F. Clemens*[,†]

[†]Laboratory for High Performance Ceramics, EMPA-Swiss Federal Laboratories for Materials Science & Technology, Überlandstrasse 129, 8600 Dübendorf, Switzerland

[‡]Federal University of Rio Grande do Sul, Laboratory of Ceramic Materials, Av. Osvaldo Aranha, 99, Porto Alegre, RS, 90035-190, Brazil

Supporting Information

ABSTRACT: This work has focused on the development of electrospun TiO_2 fiber composite photoelectrodes for hydrogen production by water splitting. For comparison, similar photoelectrodes were also developed using commercial TiO_2 (Aeroxide P25) nanoparticles (NPs). Dispersions of either fibers or P25 NPs were used to make homogenous TiO_2 films on fluorine-doped SnO_2 (FTO) glass substrates by a doctor blade (DB) technique. Scanning electron microscopy (SEM) analysis revealed a much lower packing density of the DB fibers, with respect to DB-P25 TiO_2 NPs; this was also directly reflected by the higher photocurrent measured for the NPs when irradiating the photoelectrodes at a light intensity of 1.5AM (1 sun, 1000 W/m^2). For a better comparison of fibers vs. NPs, composite photoelectrodes by dip-coating (onto FTO) TiO_2 sol-gel (SG) matrixes containing an equal amount (5 or 20 wt %) of either fibers or P25 NPs were also investigated. It emerged that the photoactivity of the fibers was significantly higher. For composites containing 5 wt % TiO_2 fibers, a photocurrent of 0.5 mA/cm^2 (at 0.23 V vs Ag/AgCl) was measured, whereas 5 wt % P25 NPs only provided 0.2 mA/cm^2. When increasing to 20 wt % fibers or NPs, the photocurrent decreased, because of the formation of microcracks in the photoelectrodes, because of the shrinkage of the sol−gel. The high photoactivity of the fiber-based electrodes could be confirmed by incident photon to current efficiency (IPCE) measurements. Remarkably, the IPCE of composites containing 5 wt % fibers was between 35% and 40% in the region of 380−320 nm, and when accounting for transmission/reflection losses, the absorbed photon to current efficiency (APCE) was consistently over 60% between 380 nm and 320 nm. The superior photoactivity is attributed to the enhanced electron transport in the electrospun fibers, with respect to P25 NPs. According to this study, it is clear that the electronic connectivity ensured by the sol−gel also contributes positively to the enhanced photocurrent.

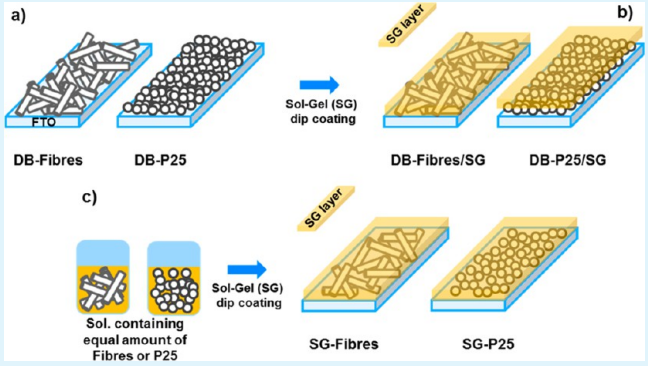

KEYWORDS: *electrospinning, fibers, TiO_2, water splitting, composite photoelectrodes*

1. INTRODUCTION

The photoelectrochemical splitting of water into hydrogen and oxygen requires semiconductors with conduction and valence bands energy straddling the electrochemical potentials of the hydrogen evolution reaction (HER, H^+/H_2) and the oxygen evolution reaction (OER, O_2/H_2O), and is capable of absorbing light with photon energies of >1.23 eV. Since the electron (e^-) and electron holes (h^+) transfer processes at the seminconductor/liquid interface are subjected to losses due to overpotentials (i.e. voltage drop, concentration gradients), the required band-gap necessary to drive water splitting is generally considered to be in the range of 1.6−2.4 eV.[1] Among the materials capable of addressing such thermodynamic requirements, a primary role is played by TiO_2, which has been extensively investigated[2−4] since the seminal work of Fujishima and Honda in 1972.[5] TiO_2 is widely regarded as an efficient, environmentally friendly, economically accessible, photostable, and biologically inert photocatalyst.[3,4] The main drawbacks of TiO_2 are (i) its rather too-large band-gap (3.0 eV for rutile and 3.2 eV for anatase), hence the possibility to harvest only a small portion (5%) of the solar energy spectrum;[3] and (ii) high recombination of photogenerated e^- and h^+.

The extension of the absorption range of TiO_2 into the visible-light range is still an ongoing issue and is generally addressed either by doping[3,6,7] or by coupling the TiO_2 with a narrower band-gap semiconductor.[4,7]

Received: August 16, 2013
Accepted: October 18, 2013
Published: October 18, 2013

Table 1. Short Description of the Different Type of Photoelectrodes Investigated within This Work

type of photoelectrode	short name	description	further comments
(i) doctor blade (DB)	DB fibers	TiO_2 fibers onto an FTO substrate	difficult to compare photoactivity of fibers and P25, because of their very different packing density
	DB-P25	TiO_2 P25 NPs onto an FTO substrate	
(ii) doctor blade (DB) and sol–gel (SG) dip coating	DB fibers/SG	TiO_2 fibers onto an FTO substrate, followed by dip coating	allowed to partially compensate the lower packing density of the fibers
	DB-P25/SG	TiO_2 P25 NPs onto FTO glass, followed by dip coating	
(iii) sol–gel (SG) dip coating	SG-0 wt % (pristine)	sol–gel with no TiO_2 fibers or P25 NPs, dip-coated onto an FTO substrate	meaningful comparison of the photoactivity of fibers and P25 for a given wt %
	SG-5 wt % fibers	sol–gel containing 5 wt % of TiO_2 fibers, dip-coated onto an FTO substrate	
	SG-5 wt % P25	sol–gel containing 5 wt % of TiO_2 P25 NPs, dip-coated onto an FTO substrate	
	SG-20 wt % fibers	sol-gel containing 20 wt % of TiO_2 fibers, dip coated onto an FTO substrate	
	SG-20 wt % P25	sol–gel containing 20 wt % of TiO_2 P25 NPs, dip coated onto an FTO substrate	

Regarding strategies to reduce recombination, one should first consider the kinetics behind water splitting. Electron transport in nanostructured porous metal-oxide semiconductors is occurring through localized energy levels within the oxide (i.e. trapping-detrapping mechanism),[8] and it is also aided by a so-called "self-doping" effect occurring on the non-illuminated region of the photoanode.[9,10] Typically, recombination occurs on the microsecond scale and thus competes with (and limits the efficiency of) the targeted photocatalytic process.[6] When considering photoelectrochemical water splitting, there is general agreement that a more efficient transfer of h^+ from the semiconductor photoanode to water (considered to be the rate-determining step) is necessary to tackle recombination.[11,12] Similarly, increasing the transport of e^- through the photoanode to the current collector would be beneficial. Because of the small particles size and the higher surface area, nanomaterials may allow for more-efficient charge collection[13] and are at the core of the research in photocatalysis and renewable energy applications.[14] On the other hand, it has also been observed that TiO_2 nanoparticles in contact with the electrolyte may lead to an increase of charge recombination at the surface of the film, because of the formation of highly reducible radical species that act as electron scavengers.[15] Therefore, it is very important to properly select the type and morphology of the nanomaterial and optimize its charge transport properties. As a significant example, Ghadiri et al.[16] reported an enhanced electron collection efficiency (i.e., an electron lifetime 3–4 times larger and electron transport that occurs twice as fast) for TiO_2 nanofibers, with respect to TiO_2 spherical nanoparticles in dye-sensitized solar cells (DSSCs). Similar conclusions were reached by Choi et al.,[17] who studied suspensions of electrospun TiO_2 nanofibers for photocatalytic water splitting; their superiority over TiO_2 nanoparticles was attributed to the mesoporosity and the alignment of the fibers,[18] causing a more-efficient charge separation and facilitating interparticle charge transfer along the fibrous network.

The development of electrospun TiO_2 fiber[19] composite photoelectrodes for hydrogen production by water splitting is the final aim of this investigation. Previous studies[16,17] suggest that TiO_2 fibers have the potential to minimize charge recombination and deserve further attention. The photoactivity of electrospun TiO_2 fibers doctor-bladed onto conductive fluorine-doped SnO_2 (FTO) glass substrates is here evaluated against the photoactivity of similarly prepared photoelectrodes based on commercial P25 TiO_2 nanoparticles. To the best of our knowledge, a direct comparison between TiO_2 fibers and nanoparticles for water splitting, adopting a photoelectrochemical cell (PEC) configuration, has not yet been reported. Because of the different microstructure (i.e., packing density) of fibers and nanoparticle photoelectrodes, TiO_2-based sol–gel composites photoelectrodes containing a fixed amount (0, 5, and 20 wt %) of fibers or P25 nanoparticles have been also investigated. Such a study also allows to evaluate a possible synergy with SG fibers and SG nanoparticles composites, since mesoporous TiO_2 obtained by sol–gel synthesis is known to generate a good photocurrent response toward water splitting.[20,21]

2. EXPERIMENTAL PROCEDURE

2.1. Synthesis and Processing of Electrospun TiO_2 fibers. The experimental procedure to produce electrospun fibers is based on a sol–gel synthesized from an alkoxide in the presence of acetic acid. The materials used in this study were supplied by Sigma–Aldrich without further purification. Titanium(IV) tetraisopropoxide (Ti-$(OPr^i)_4$) was used as a precursor for the fibers. A 10 wt % solution of poly(vinylpyrrolidone) (PVP, molecular weight of $M_w = 1.3 \times 10^6$ g/mol) was prepared by dissolving the PVP in anhydrous ethanol (under magnetic stirring until complete homogenization was achieved). Typically, Ti$(OPr^i)_4$ and acetic acid were added together in a 1:1 volume ratio, and, after 15 min, an amount of PVP solution equivalent to the total volume of the Ti$(OPr^i)_4$ and acetic acid mixture was added. This sol was allowed to rest in darkness for 24 h, before being electrospun using the following parameters: high voltage (12 kV); distance from capillary needle (with an internal diameter of 0.5 mm) to the collector, 120 mm; and flow rate, 2.5 mL/h. The electrospinning process consists of loading a syringe with the sol, adjusting the flow rate of the infusion pump, connecting the capillary needle to the power supply and the collector to the ground of the electric circuit, and switching on the high-voltage power supply. The fiber formation starts when an emission voltage is reached. The fibers were then collected over a period of 30 min. To eliminate the polymer, the electrospun fibers were heat-treated at 600°C in air, at a heating rate of 1.6 °C/min and with a dwelling time of 2 h. Further details can be found elsewhere.[19]

2.2. Fabrication of TiO_2-Based Photoelectrodes. For clarity, a description of the various photoelectrodes, including the short names used to identify them within this study, is provided in Table 1, and a sketch of the photoelectrodes is also provided in Figures 1a–c. Three

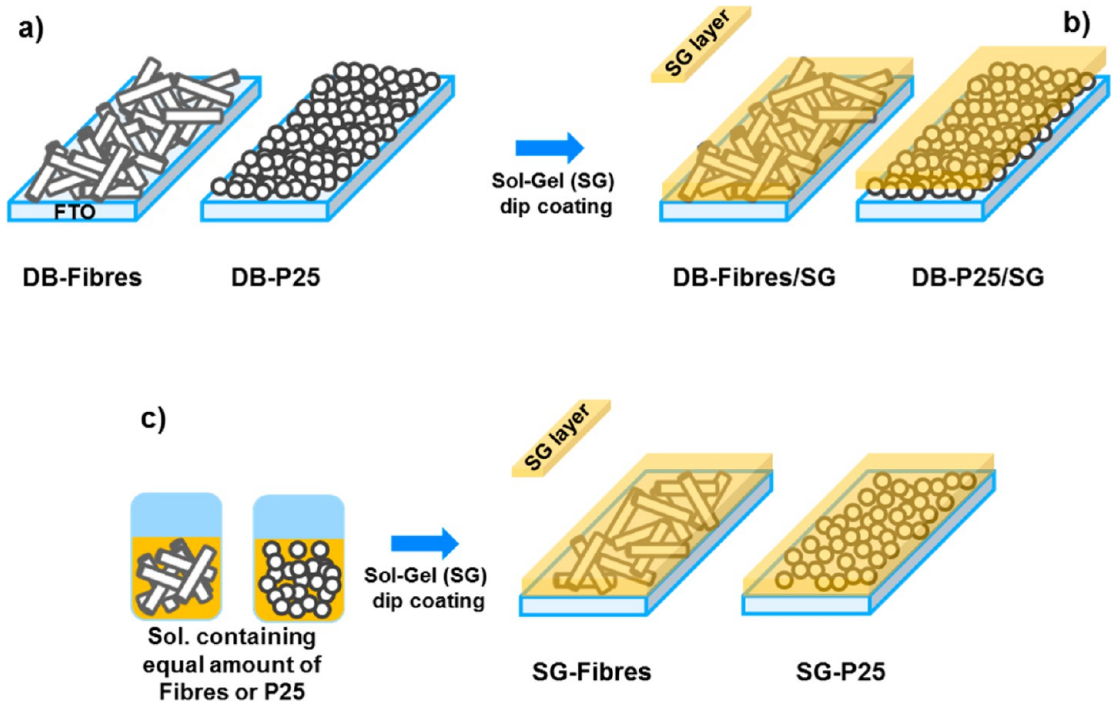

Figure 1. Sketch of the different photoelectrodes: (a) doctor-bladed (DB) fibers and DB-P25, (b) DB fibers/sol–gel dip-coating (SG) and DB-P25/SG, and (c) SG fibers and SG-P25 photoelectrodes.

different types of photoelectrodes were fabricated: (i) by doctor-blade technique (DB fibers and DB-P25), (ii) by combining the doctor-blade technique and sol–gel dip coating (DB fibers/SG, DB-P25/SG), and finally (iii) by sol–gel dip-coating (SG-0 wt %, SG-5 wt % fibers, SG-5 wt % P25, SG-20 wt % fibers, SG-20 wt % P25).

(i) Doctor-Bladed (DB) Fibers and P25 NPs (Figure 1a). Dispersions of sintered TiO_2 fibers or as-received (Aeroxide P25) commercial TiO_2 P25 NPs were fabricated by following and adapting a previously reported recipe.[22] A mass of fibers or NPs (0.8 g) was suspended in 8 g of ethanol (EtOH) with the aid of a sonication probe (Vibra Cell CV18, Sonics). A small quantity (0.2 g) of poly(vinyl butyral) (PVB, Mowital B 30H, Omya) were mixed with 3.0 g of anhydrous Terpineol (Sigma–Aldrich) and then added to the TiO_2–EtOH mixture while sonicating. The suspensions were finally left to stir overnight before being doctor-bladed on FTO glass substrates (Pilkington NSG TEC 8A, Xop Física). The FTO substrates were cleaned by sonication in isopropanol for 10 min, then rinsed with distilled water and EtOH and finally dried under an air flow before doctor blading.

(ii) Sol–Gel (SG) and Doctor-Bladed Fibers or P25 NPs Composites (Figure 1b). Such composite photoelectrodes were fabricated by firstly doctor blading the TiO_2 fibers or P25 NPs as described above, then by dip-coating a sol-gel layer on top of the doctor-bladed (tape-casted) layer. The sol–gel was prepared as follows. A quantity (2.84 mL) (9.6 mmol) of titanium tetraisopropoxide ($Ti(OPr^i)_4$, Merck) were mixed in 2.84 mL (50 mmol) of acetic acid (Sigma–Aldrich) and kept under magnetic stirring for 10 min. The sol was then kept in darkness for 15 min,[19] before adding 0.8 mL (7.8 mmol) of acetylacetone (acac, Sigma–Aldrich), 0.1 mL of Triton-x-100 (Sigma–Aldrich), and a solution made of 0.32 g of PVB (5 wt %) dissolved in 8 mL of dry EtOH. The obtained sol was aged in darkness for 6 h before performing the dip coating (Compact DipMaster 50 Dip Coater, Chemat Scientific, Inc.) The following parameters were used: 50 mm/min for substrate dipping and withdrawal speed, 30 s as dipping time.

(iii) Sol-Gel (SG) Containing 0, 5, 20 wt % of TiO_2 Fibers or P25 NPs Composites (Figure 1c). Pristine, as well as 5 and 20 wt % fibers or P25–sol–gel photoelectrodes were prepared by dip-coating a sol–gel layer, prepared as described above, onto bare and cleaned FTO substrates. In the case of SG fibers or SG-P25 NP photoelectrodes, the fibers or the nanoparticles were incorporated into the sol by adding them to the PVB solution in EtOH and dispersing them with an ultrasonic probe (typically ultrasounds were applied for 20 min).

All the photoelectrodes prepared according to procedures (i), (ii), and (iii) previously described, were dried (aged) for 24 h and then calcined at 500 °C in air, at a heating rate of 1.6 °C/min and with a dwelling time of 2 h.

2.3. Characterization. *2.3.1. Morphology, Microstructure, Crystallinity, and Surface Area of Photoelectrodes. SEM, XRD, and BET Analysis.* The morphology and the microstructure of the photoelectrodes were analyzed by scanning electron microscopy (SEM), either using a TS5136 MM (Tescan) or a field-emission Nova NanoSEM 230 (Nova FEI) for magnifications above 15 000×. SEM and profilometry (Alpha Step D-120, KLA Tencor) were also used to determine the thickness of the photoelectrodes. Crystal phases were detected by X-ray diffraction (XRD) analysis, performed either on TiO_2 fibers or P25 NPs as powders (Bragg–Brentano mode, θ–2θ) or directly on thin films (grazing-angle X-ray diffraction (GAXRD), geometry, $\omega = 1°$), using a Panalytical X'Pert Pro instrument (Cu Kα_1, λ = 1.5406 Å), whereas the Brunauer–Emmett–Teller (BET) surface area of the photoelectrodes was determined (on powders) using a SA3100 (Coulter) instrument.

2.3.2. Photoelectrochemical Characterization. Photocurrent Measurements. The photocurrent measurements were performed using a three-electrode system and a so-called Cappuccino cell[23] filled with 10 mL of 1M KOH solution (pH 13.8) and connected to a potentiostat (Voltalab80 PGZ 402, Radiometer Analytical). The TiO_2 photoanode was set as the working electrode, whereas a platinum plate (XM120, Radiometer Analytical) was used as the counter electrode and Ag/AgCl/3M-KCl (XR300, Radiometer Analytical) was used as the reference electrode. A potential bias was applied from −900 mV to +900 mV, vs the Ag/AgCl reference electrode, at a scan rate of 20 mV/s. The working electrode within the Cappuccino cell was irradiated by a xenon lamp (solar simulator, Oriel Lamp by L.O.T.–Oriel AG), at an intensity corresponding to 1.5AM (1 sun, 1000 W/m^2), and the resulting photocurrent was recorded.

Incident Photon to Current Efficiency (IPCE), Optical Analysis (UV-Visible), and Absorbed Photon to Current Efficiency (APCE) Measurements. Incident photon to current efficiency (IPCE) investigations were also performed using a xenon lamp (by L.O.T.–

Oriel AG) as light source and a monochromator (Omni-λ 300, L.O.T.−Oriel AG) to select the appropriate wavelength (λ) of irradiation. A typical experiment consistent in sweeping the wavelength of the light from 650 nm to 300 nm (1 nm step) on a TiO_2 photoanode immersed in 1M KOH solution. A Keithley 2400 source meter was used to provide a bias of 0.23 V vs Ag/AgACl and to measure the photocurrent, $J_{Photo}(\lambda)$. The power of the irradiating source, $P(\lambda)$, was recorded using a ThorLabs PM100USB power/energy meter and the IPCE(λ) values (expressed as a percentage) were then obtained as

$$\mathrm{IPCE}(\lambda)\ (\%) = 1240 \times \frac{J_{\mathrm{Photo}}(\lambda)\ (\mu\mathrm{A\ cm^{-2}})}{\lambda P(\lambda)\ (\mathrm{nm\ W\ m^{-2}})} \quad (1)$$

UV-visible analysis, using a UV 3600 Spectrophotometer (Shimadzu) was also performed to determine the transmittance and the diffuse reflectance of the various photoelectrodes (T_{TiO_2}, R_{TiO_2}), and the FTO substrate (T_{FTO}, R_{FTO}), ranging from λ = 650 nm to λ = 200 nm (sampling interval of 1 nm). The optical absorption $A(\lambda)$ and the absorbed photon to current efficiency (APCE) were then determined from[24]

$$A(\lambda) = 1 - \left(\frac{T_{TiO_2}}{1 - R_{TiO_2}}\right)\left(\frac{1 - R_{FTO}}{T_{FTO}}\right) \quad (2)$$

$$\mathrm{APCE}(\lambda)\ (\%) = \frac{\mathrm{IPCE}(\lambda)\ (\%)}{A(\lambda)} \quad (3)$$

3. RESULTS AND DISCUSSION

3.1. TiO_2 Doctor-Bladed Fibers and DB-P25 Photoelectrodes. The fibers sintered at 600 °C have a BET surface area of 32 m^2/g, which is in good agreement with previous studies;[19] such a value is significantly lower than the surface area of P25 NPs calcined at 500 °C, 47 m^2/g (that of as-received P25 NPs was 48 m^2/g). Furthermore, it can be appreciated from the GAXRD analysis in Figure 2 that both DB fibers and DB-P25 films consist of a mixture of anatase and rutile crystals,[25] which is an ideal case leading to enhanced charge separation across the phase junctions.[26−28] Electron paramagnetic resonance (EPR) spectroscopy[26] and recent theoretical[28] studies strongly suggest that such charge separation is due to a photogenerated electron moving from the conduction band of rutile to the conduction band (or to a trapping site below the conduction band) of anatase. As a result, the photogenerated electron−hole pair is physically separated (i.e., the hole is located at the valence band of rutile) and, therefore, is less prone to recombine. The powder XRD analysis of TiO_2 fibers and P25 NPs is also reported in Figure 2. Both powders mainly consist of anatase ($\geq$ 70%) and the same composition is preserved on thin film DB-P25 photoelectrodes. Interestingly the rutile content in the DB-fiber photoelectrodes (~60%) is higher than in the fibers ($\leq$ 30%) analyzed by powder XRD; it appears as if the FTO glass substrate would somehow lower the temperature required for the anatase-to-rutile phase transition in the electrospun fibers. It may be that exposing the already-sintered fibers to a carbon-rich suspension (i.e., an organic solvent and a binder are used for the preparation of the suspension for the doctor blade) and then re-firing the DB fibers promotes the formation of a higher number of oxygen vacancies, which is ultimately better accommodated within a rutile structure.[29]

Further information on the photoelectrodes is provided by SEM analysis. Clearly, the DB-fiber photoelectrode (Figure 3a) is not as densely packed as the DB-P25 photoelectrode (Figure 3b), and several uncovered patches exposing the FTO layer underneath can be clearly seen in the DB fibers film (Figure

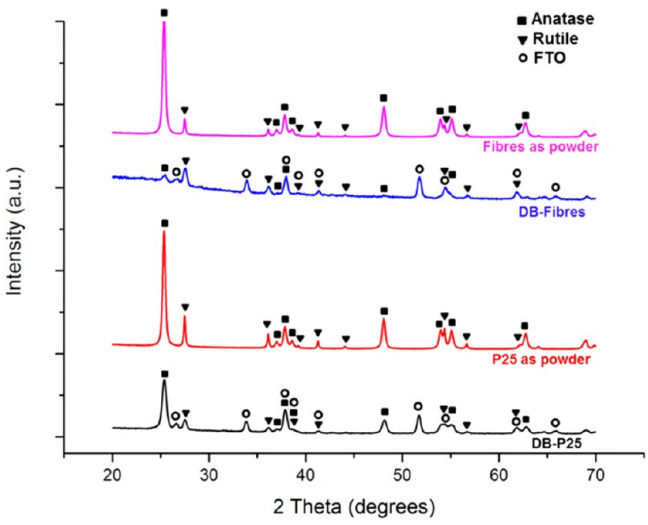

Figure 2. Comparison between XRD analysis of TiO_2 fibers and P25 powders and GAXRD analysis of thin films of DB fiber and DB-P25 photoelectrodes.

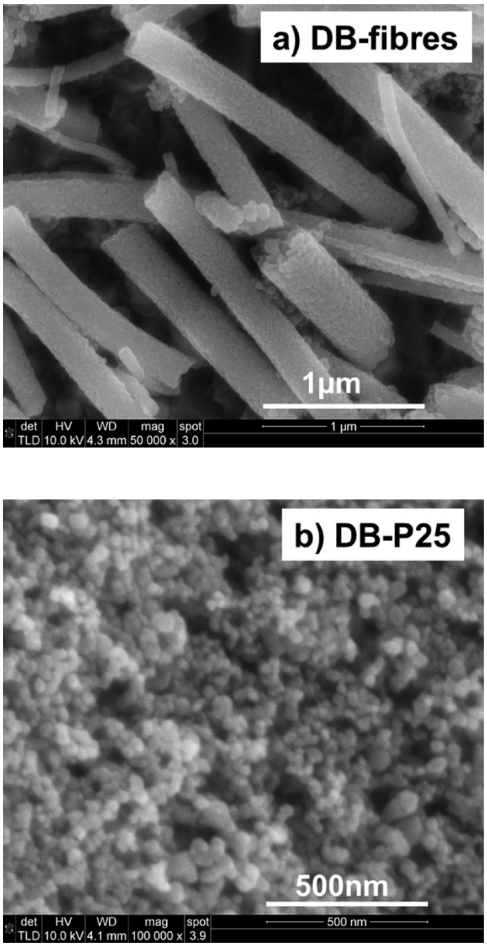

Figure 3. Top view of (a) DB fibers and (b) DB-P25 photoelectrodes prepared by doctor-blading TiO_2 fibers or P25 NPs on a FTO glass substrate.

3a). Therefore, it is not surprising that the photocurrent density, $J_{Photo}(\lambda)$ (see Figure 4), is significantly lower for DB

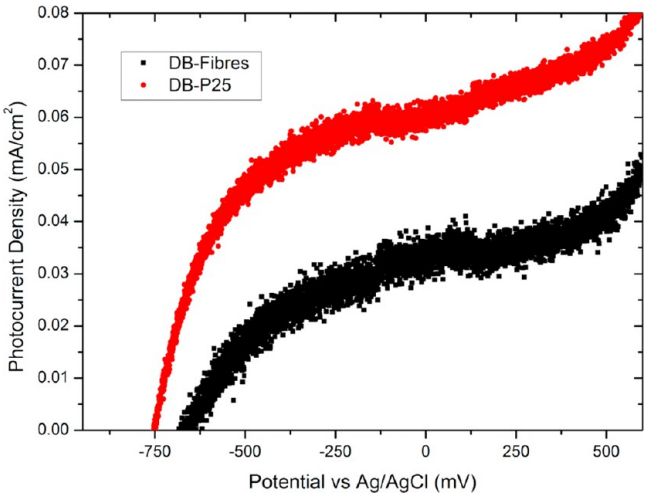

Figure 4. Photocurrent measurements, performed at a light intensity of 1.5AM in 1M KOH, on DB fibers and DB-P25 photoelectrodes.

fibers (30 μA/cm^2 at 0.23 V vs Ag/AgCl (i.e. 1.23 V vs RHE)) than for DB-P25 (60 μA/cm^2 at 0.23 V vs Ag/AgCl). Other factors that may be also responsible for the different photoactivities of DB fibers and DB-P25 thin films are (i) their different anatase content, highlighted in Figure 2, and (ii) their surface area.

3.2. DB Fibers/SG and DB-P25/SG Composite Photoelectrodes. Based on results discussed in section 3.1, the following step has been taken to tackle the different packing density of the fibers and the P25 NPs in order to clarify the reasons behind their (apparently) different photocurrent densities (see Figure 4). Hence, the DB photoelectrodes (schematically depicted in Figure 1a) were also covered by a dip-coated sol–gel layer (as sketched in Figure 1b).

Despite the presence of cracks due to the shrinkage of the sol–gel network, it is clear from SEM analysis (see Figure 5a) that the exposure of the FTO layer to the electrolyte, which is particularly significant for the previously discussed DB fibers (Figure 3a), is minimized by the introduction of the sol–gel layer. It is also interesting to observe that, because of the higher packing density of P25 NPs, the sol–gel layer (Figure 5b) could not penetrate the P25 NPs network and was found to be on top of the highly homogeneous NPs layer (i.e., no areas with FTO glass exposed and good dispersion of the NPs), as also schematically shown in Figure 1b. Therefore, by dip-coating a sol–gel layer of TiO_2 on top of the DB fibers and DB-P25 films, it has been possible to investigate the influence of porous and dense structure with different DB fibers and DB-P25 contents. Figure 6 shows that the photocurrent densities of the infiltrated structures increase significantly. Similar results—150 μA/cm^2 for DB fibers/SG and 135 μA/cm^2 for DB-P25/SG (at 0.23 V vs Ag/AgCl)—could be observed.

3.3. SG-0 wt %, SG-5 wt %, SG-20 wt % Fibers or P25 Composite Photoelectrodes. The infiltration of the doctor-bladed structures with the TiO_2 sol (Figure 1b) still has the disadvantage of giving composite photoelectrodes with different fibers and powder contents. Therefore, composite photoelectrodes made by dip-coating (onto FTO glass substrates), based on TiO_2 sol–gel (SG) matrix containing an equal

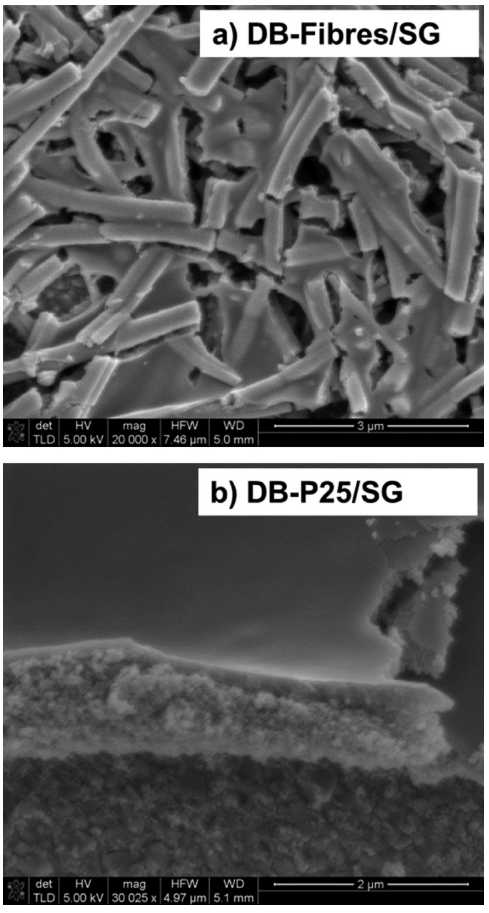

Figure 5. Top view of (a) DB fibers/SG and (b) DB-P25/SG photoelectrodes prepared by doctor-blading TiO_2 fibers or P25 NPs on a FTO glass substrate and then dip coating a TiO_2 sol–gel layer on top of the fibers or P25 NPs.

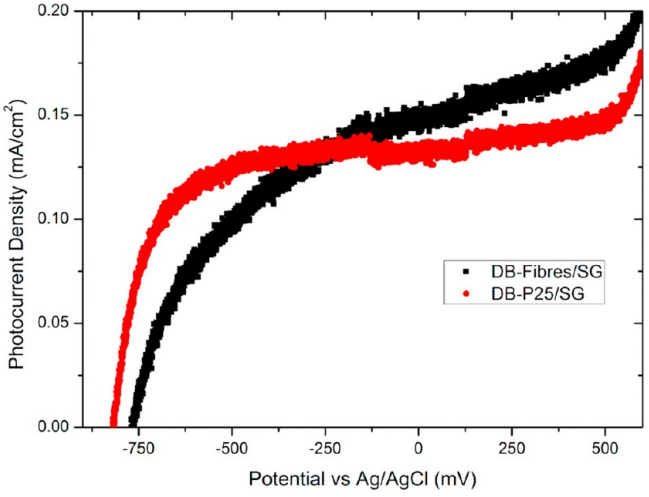

Figure 6. Photocurrent measurements, performed at a light intensity of 1.5AM in 1M KOH, on DB fibers/SG and DB-P25/SG photoelectrodes.

amount (5 or 20 wt %) of either fibers or P25 NPs, were also investigated (see the sketch shown in Figure 1c). The thickness of such photoelectrodes was determined to be in the range of 0.8–1 μm. The GAXRD analysis (Figure 7) indicates the presence of both anatase and rutile crystals in all of the

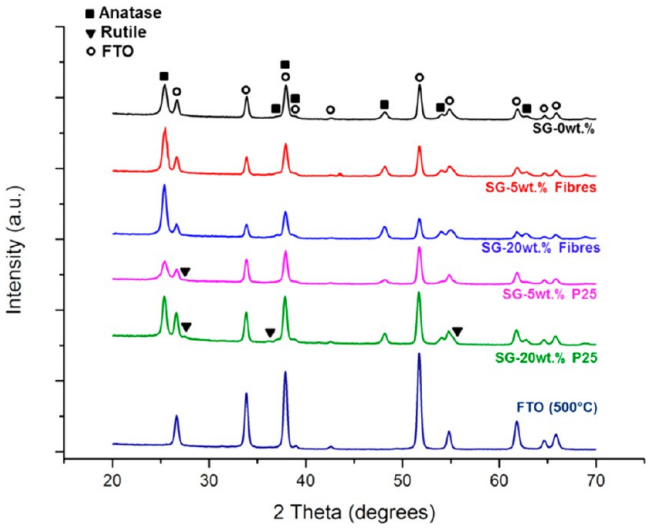

Figure 7. GAXRD analysis on different composite photoelectrodes prepared by mixing a fixed amount (5 and 20 wt %, or 0 wt % for pristine SG) of TiO_2 fibers or P25 NPs into a sol−gel (SG) matrix.

photoelectrodes. Similar results are also observed for SG-0 wt % (i.e., pristine SG, with no fibers or P25 NPs). Particularly, the anatase content is estimated to be in the order of 85%−90% in all SG-0 wt %, SG-5 wt % fibers, SG-5 wt % P25, SG-20 wt % fibers, and 20 wt % P25 photoelectrodes. It is also interesting to consider the analysis of the surface area of the different photoelectrodes.

The pristine SG-0 wt % has a surface area of 22 m^2/g. Because of the interaction between the sol−gel matrix and the fibers, i.e., the external area of the fibers is covered by the sol−gel, as shown by SEM analysis in Figures 8a and 8b, the composite photoelectrodes containing the fibers have a lower surface area, 18 m^2/g for SG-5 wt % fibers and 14 m^2/g for SG-20 wt % fibers. Instead, a different situation is observed for the SG-P25 structures; the P25 nanoparticles roughen the surface of the film (see Figures 9a and 9b) and, hence, their large surface area is still partially exposed. For example, the surface area of SG-20 wt % P25 is 26 m^2/g, slightly larger than the area of the pristine photoelectrode SG-0 wt %.

Another aspect, emerging from the SEM analysis, is that the SG-0 wt % structure exhibits good porosity and interconnection between TiO_2 particles (see Figures 10a and 10b). Such features are also preserved when incorporating the fibers or the P25 into the sol−gel (for an example, see Figure S-1 in the Supporting Information, which is an SEM image of a SG-5 wt % fibers photoelectrode). However, a significant number of larger cracks is induced whenever inserting 20 wt % of fibers into the sol−gel matrix (Figures 8a and 8b, because of the shrinkage of the SG during the calcination process.

From photocurrent density measurements (Figure 11), it clearly emerges that the photoactivity of the SG fibers (5 and 20 wt %) is greater than that for the SG-P25 (5 and 20 wt %) composites. The best performances are observed for the SG-5% fibers photoelectrodes: 0.5 mA/cm^2 at 0.23 V vs Ag/AgCl, which is more than twice the photocurrent generated by the SG-5% P25 composites (0.2 mA/cm^2). The photoactivity of composite photoelectrodes with a fiber content of 20 wt % is clearly affected (reduced) by the presence of cracks. Similarly, the photoactivity of SG-20 wt % P25 decreases; in this case (Figures 9a and 9b), cracks are not so significant as in SG-20

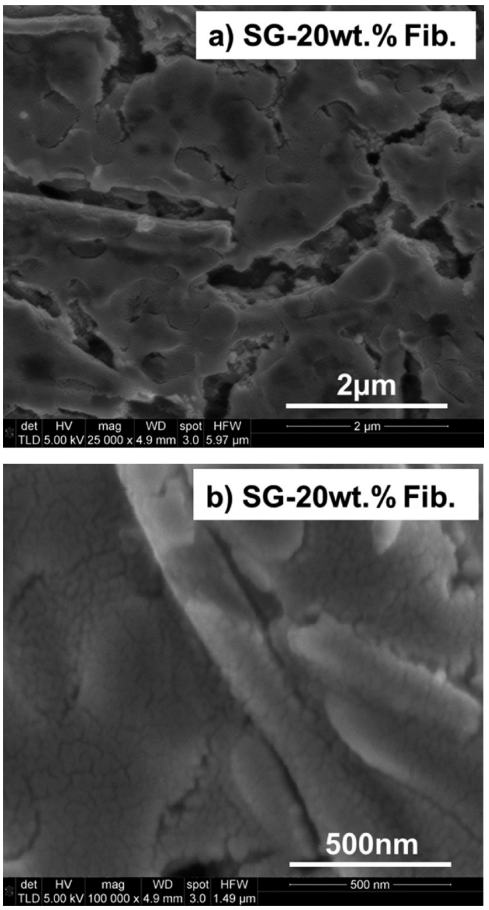

Figure 8. Top view of (a) SG-20 wt % fibers photoelectrode and (b) high-magnification details showing the fibers covered by the sol−gel matrix and the presence of cracks within the photoelectrode.

wt % fibers (Figures 8a and 8b); hence, the poor photoactivity may be a consequence of an increased recombination at the interface between P25 NPs and the SG matrix.

Nevertheless, despite the lower photoactivity of SG-20 wt % composites, the superiority of the fibers, with respect to P25 NPs, is confirmed, to the point that the SG-20 wt % fibers photoelectrodes also outperform the SG-5% P25 photoelectrodes (see Figure 11). It can be inferred that the lower surface area of the SG-fibers composites is very well compensated by the better interconnectivity and the fibrous network. In fact, with respect to water splitting, it appears that a good interconnectivity in the nanostructures, associated with the sol−gel due to the chemical bonds established between the TiO_2 units forming the sol-gel network, is more important than having a large surface area. Similarly, such interconnectivity is preserved in fibers electrospun from a sol−gel matrix, and that explains their high photoactivity. It is worth mentioning that the best photoactivity, 0.6 mA/cm^2 at 0.23 V vs Ag/AgCl, is shown by the SG-0 wt % (pristine SG) photoelectrode (Figure 11). Clearly, the idea of combining fibers with a sol−gel matrix, both having good electron transport properties, is very interesting, but also poses a new challenge, such as the recombination occurring at the interfacial SG fibers and more generally in SG-composites photoelectrodes.

To gain a deeper understanding on the performances of the SG-composite photoelectrodes as a function of wavelength, IPCE, UV-Vis, and APCE measurements were also performed.

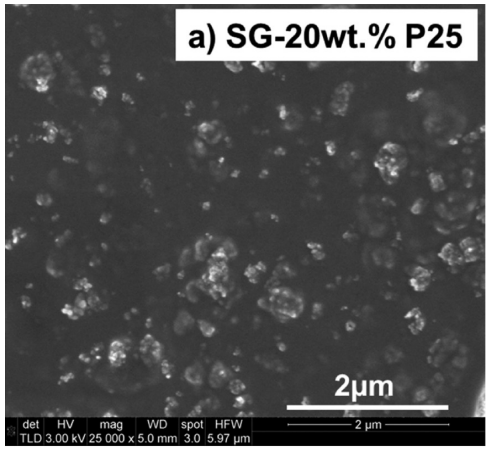

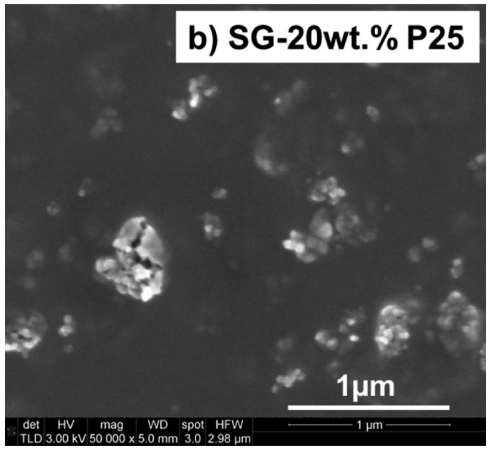

Figure 9. Top view of (a) SG-20 wt % P25 photoelectrode and (b) high-magnification details showing the presence of clusters of P25 NPs on the top of the sol–gel matrix.

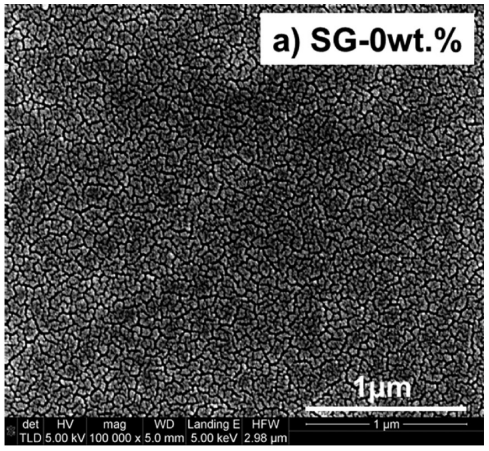

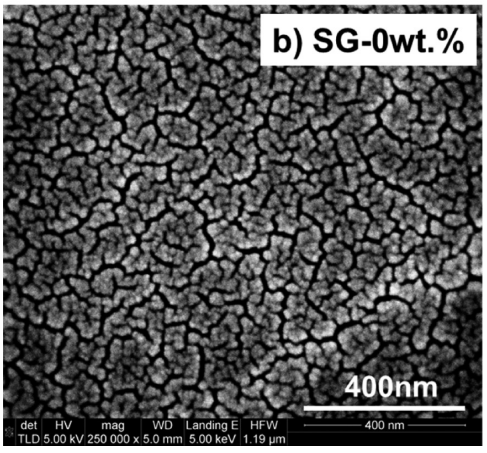

Figure 10. Top view of (a) SG-0 wt % (i.e., pristine SG) photoelectrode and (b) high-magnification details showing the porosity of the sol–gel matrix.

The IPCE spectra recorded at 1.23 vs RHE are reported in Figure 12. Remarkably, the IPCE of SG-5 wt % fibers is in the range of 20%–45% in the 360–320 nm region of the light spectrum and it is very similar to the IPCE registered for SG-0 wt % (pristine sol–gel). Instead, SG-20 wt % fibers photoelectrodes have an IPCE of ~25% over the same region, 360–320 nm, suggesting that a higher recombination occurs when the amount of fibers is increased, and also confirming that the presence of cracks (Figures 8a and 8b) negatively affect the photoactivity. Poor photoactivity and IPCE values that are constantly well below 20% are instead observed for SG-P25 composites. By accounting for transmission/reflection losses (see Figure SI-2 in the Supporting Information for an overview of the optical absorbance of the photoelectrodes), it is possible to obtain the APCE% (see Figure 13). The SG-5 wt % fibers composite exhibits APCE values close to 100%—more precisely, from 100% to 60% over the region of 380–320 nm. When increasing the fiber content to 20%, the APCE decreases to ~35%–40% in the 380–320 nm region. It is interesting to observe that the SG-5 wt % P25 photoelectrodes have performances similar to that of SG-5 wt % fibers at 380 nm and above, whereas the APCE is constantly 30%–35% below 370 nm. Instead, SG-20 wt % P25 composites have an APCE of ~15%–20% over the 380–320 nm region. The superior photoactivity of SG-fibers composites is attributed to the good electron transport properties of both the sol–gel and the fibers.

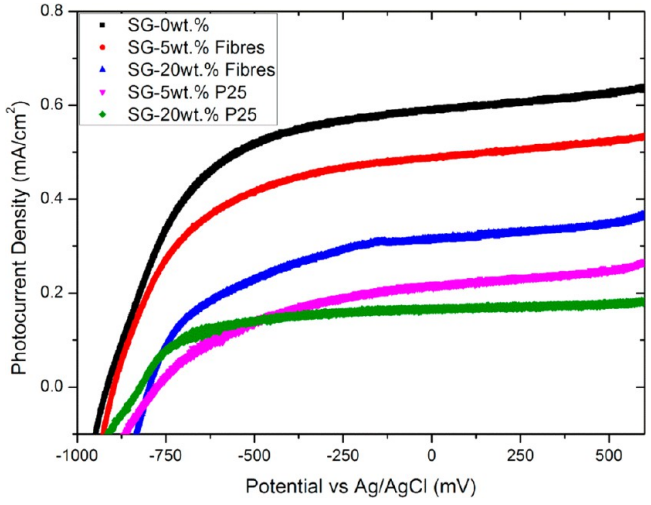

Figure 11. Photocurrent measurements performed at a light intensity of 1.5AM in 1M KOH, SG and SG-fibers, as well as SG-P25 composite photoelectrodes.

4. CONCLUSIONS

The work presented has been focused on the study of different TiO_2-based photoelectrodes and the evaluation of their photoactivity toward water splitting. In particular, two different morphologies, (electrospun) TiO_2 fibers and commercial nanoparticles (NPs), have been investigated. At first, it appears

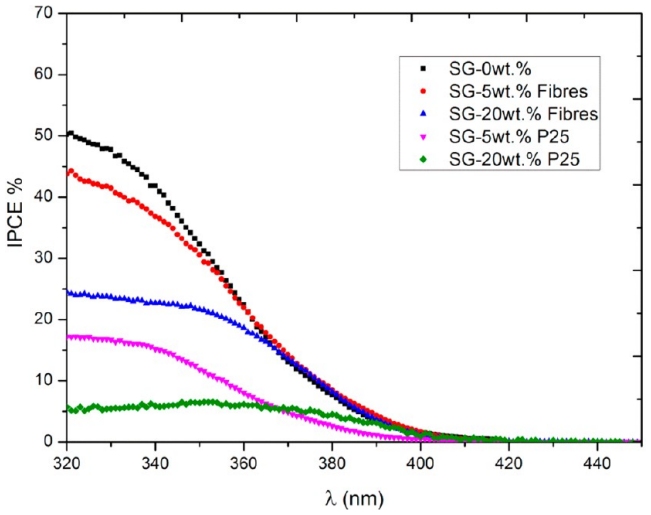

Figure 12. IPCE measurements performed on SG and SG-fibers, as well as SG-P25 composite photoelectrodes.

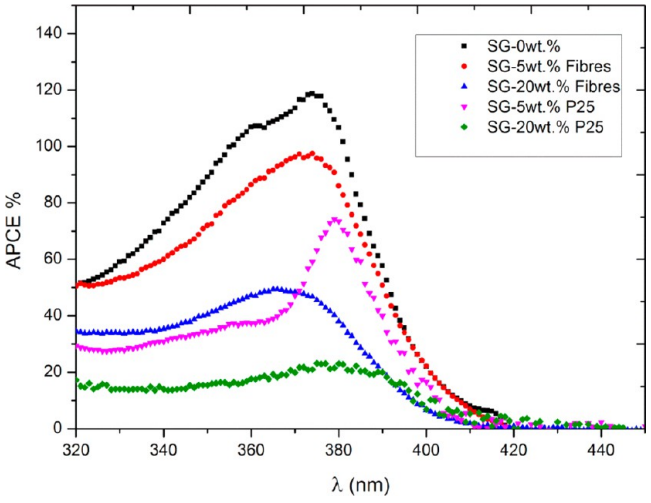

Figure 13. APCE measurements (i.e., IPCE corrected for transmittance and reflectance losses) performed on SG and SG-fibers, as well as SG-P25 composite photoelectrodes.

that the P25 NPs doctor-bladed onto a conductive substrate exhibited better performance than similarly prepared fiber photoelectrodes (photocurrent density of 60 μA/cm^2 vs 30 μA/cm^2, respectively); however, their different packing density must be taken into account for a fair comparison. Such investigation was carried out by preparing composite photoelectrodes containing a fixed amount of either fibers or P25 NPs embedded into a sol–gel (SG) matrix. It clearly emerged that electrospun fibers exhibit superior photoactivity than P25 NPs (as an example, SG-5 wt % fibers could provide up to 0.5 mA/cm^2, whereas SG-5 wt % P25 gave a photocurrent density of 0.2 mA/cm^2), because of their ability to sustain the transport of electrons throughout their microstructure, hence the good interconnectivity between the grains that comprise the fibrous network. Instead, such a feature is absent in P25 NPs, which therefore performs poorly as a photoelectrode for water splitting. This is the first report on a direct comparison between the photoactivity of electrospun TiO_2 fibers and P25 NPs under a PEC configuration, and it can be concluded that, with regard to water splitting, it is far more important to optimize the interconnectivity and the transport of photogenerated carriers throughout the photoelectrodes than to have a high surface area. Because of recombination, likely occurring at the fiber/fiber interface, NP/NP interface, or at the interface between fiber or NP and the sol–gel matrix (SG), the pristine SG (i.e., no fibers or P25 NPs) exhibits the highest photoactivity of all the photoelectrodes. A possible solution would be to sinter the photoelectrodes at higher temperature to establish a better network by sintering necks; on the other hand, the anatase content decreases (eventually disappeared) at high temperatures and it would be important to preserve a mixture of anatase and rutile, to maximize the photoactivity.[26−28] Having established that fibers can enhance the electron transport properties of a photoelectrode, future work and efforts will be dedicated to minimize the presence of cracks, detrimental for the photoactivity, in composite photoelectrodes and on the synthesis of oriented nanofibers or nanotubes[30] to maximize packing density without losing the interconnectivity between the grains of the photoactive material.

■ ASSOCIATED CONTENT

Ⓢ Supporting Information

SEM analysis of a typical SG-5 wt % fibers photoelectrode and optical absorption (used to calculate the APCE) of SG, SG fibers, and SG-P25 composite photoelectrodes. This material is available free of charge via the Internet at http://pubs.acs.org.

■ AUTHOR INFORMATION

Corresponding Authors

*E-mail: domenico.regonini@empa.ch.
*E-mail: frank.clemens@empa.ch.

Notes

The authors declare no competing financial interest.

■ ACKNOWLEDGMENTS

The authors gratefully thank the financial support from Brazilian Swiss Joint Research Programme (No. BSJRP 0112-11). Financial support for research equipment by the Swiss National Science Foundation under Project No. R′Equip 206021-121306 (Fundamental Aspects of Photocatalysis and Photoelectrochemistry/Basic Research Instrumentation for Functional Characterization) is also kindly acknowledged. K. G.-S. was financially supported by the VELUX Foundation (Project No. 790). Dr. Artur Braun (EMPA) is kindly acknowledged for valuable discussions and for providing experimental facilities. The photoelectrochemical (Cappuccino) cell was built by Peter Wyss and Marc Zollinger (EMPA Machine Shop) after the original design provided by the Laboratory for Photonics and Interfaces, EPFL Lausanne. The IPCE instrument was developed by Dr. Fabio La Mattina and André Kupferschmid (EMPA).

■ REFERENCES

(1) Walter, M. G.; Warren, E. L.; McKone, J. R.; Boettcher, S. W.; Mi, Q.; Santori, E. A.; Lewis, N. S. *Chem. Rev.* **2010**, *110*, 6446–6473.
(2) Linsebigler, A. L.; Lu, G.; Yates, J. T. *Chem. Rev.* **1995**, *95*, 735–758.
(3) Bak, T.; Nowotny, J.; Rekas, M.; Sorrell, C. C. *Int. J. Hydrogen Energy* **2002**, *27*, 991–1022.
(4) Ni, M.; Leung, M. K. H.; Leung, D. Y. C.; Sumathy, K. *Renew. Sust. Energy Rev.* **2007**, *11*, 401–425.
(5) Fujishima, A.; Honda, K. *Nature* **1972**, *238*, 37–38.

(6) Fujishima, A.; Zhang, X.; Tryk, D. *Surf. Sci. Rep.* **2008**, *63*, 515−582.
(7) Chen, X.; Mao, S. S. *Chem. Rev.* **2007**, *107*, 2891−2959.
(8) Anta, J. A. *Curr. Opin. Colloid Interface Sci.* **2012**, *17*, 124−131.
(9) Wahl, A.; Augustynski, J. *J. Phys. Chem. B* **1998**, *102*, 7820−7828.
(10) Solarska, R.; Augustynski, J.; Sayama, K. *Electrochim. Acta* **2006**, *52*, 694−703.
(11) Cowan, A. J.; Tang, J.; Leng, W.; Durrant, J. R.; Klug, D. R. *J. Phys. Chem. C* **2010**, *114*, 4208−4214.
(12) Cowan, A. J.; Barnett, C. J.; Pendlebury, S. R.; Barroso, M.; Sivula, K.; Gratzel, M.; Durrant, J. R.; Klug, D. R. *J. Am. Chem. Soc.* **2011**, *133*, 10134−40.
(13) Kudo, A.; Miseki, Y. *Chem. Soc. Rev.* **2009**, *38*, 253−278.
(14) Chen, X.; Li, C.; Grätzel, M.; Kostecki, R.; Mao, S. S. *Chem. Soc. Rev.* **2012**, *41*, 7909−7937.
(15) Augustynski, J.; Solarska, R. *Catal. Sci. Technol.* **2013**, *3*, 1810−1814.
(16) Ghadiri, E.; Taghavinia, N.; Zakeeruddin, S. M.; Grätzel, M.; Moser, J.-E. *Nano Lett.* **2010**, *10*, 1632−1638.
(17) Choi, S. K.; Kim, S.; Lim, S. K.; Park, H. *J. Phys. Chem. C* **2010**, *114*, 16475−16480.
(18) Kayes, B. M.; Atwater, H. A.; Lewis, N. S. *J. Appl. Phys.* **2005**, *97*, 114302.
(19) Alves, A. K.; Berutti, F. A.; Clemens, F. J.; Graule, T.; Bergmann, C. P. *Mater. Res. Bull.* **2009**, *44*, 312−317.
(20) Waldner, G. *Int. J. Photoenergy* **2003**, *5*, 115−122.
(21) Hartmann, P.; Lee, D.-K.; Smarsly, B. M.; Janek, J. *ACS Nano* **2010**, *4*, 3147−3154.
(22) Tsekouras, G.; Miyashita, M.; Yung Kent, K.; Wey Yang, T.; Mozer, A. J.; Amal, R.; Mori, S.; Wallace, G. G. *IEEE J. Sel. Top. Quantum Electron.* **2010**, *16*, 1641−1648.
(23) Van de Krol, R.; Gratzel, M. In *Electronic Materials: Science & Technology*, 1st Edition; Springer: New York, 2012.
(24) Hisatomi, T.; Dotan, H.; Stefik, M.; Sivula, K.; Rothschild, A.; Grätzel, M.; Mathews, N. *Adv. Mater.* **2012**, *24*, 2699−2702.
(25) Alves, A. K.; Berutti, F. A.; Bergmann, C. P. *MRS Proc.* **2012**, *1442*, DOI: 10.1557/opl.2012.1365.
(26) Hurum, D. C.; Agrios, A. G.; Gray, K. A.; Rajh, T.; Thurnauer, M. C. *J. Phys. Chem. B* **2003**, *107*, 4545−4549.
(27) Kho, Y. K.; Iwase, A.; Teoh, W. Y.; Mädler, L.; Kudo, A.; Amal, R. *J. Phys. Chem. C* **2010**, *114*, 2821−2829.
(28) Scanlon, D. O.; Dunnill, C. W.; Buckeridge, J.; Shevlin, S. A.; Logsdail, A. J.; Woodley, S. M.; Catlow, C. R. A.; Powell, M. J.; Palgrave, R. G.; Parkin, I. P.; Watson, G. W.; Keal, T. W.; Sherwood, P.; Walsh, A.; Sokol, A. A. *Nat. Mater.* **2013**, *12*, 798−801.
(29) Hanaor, D. A. H.; Sorrell, C. C. *J. Mater. Sci.* **2010**, *46*, 855−874.
(30) Regonini, D.; Bowen, C. R.; Jaroenworaluck, A.; Stevens, R. *Mater. Sci. Eng., R.* **2013**, DOI: 10.1016/j.mser.2013.10.001.